Vision Research 215 (2024) 108347

Contents lists available at ScienceDirect

Vision Research

journal homepage: www.elsevier.com/locate/visres

Monocular and binocular mechanisms detect modulations of dot density and dot contrast

Kristina Zeljic *, Michael J. Morgan, Joshua A. Solomon

Centre for Applied Vision Research, City, University of London, London, UK

ARTICLE INFO

Keywords:
Texture
Density
Contrast
Signal detection
Dichoptic
Inverse-cyclopean

ABSTRACT

Strong reciprocity has been demonstrated between (1) spatial modulations of dot density and modulations of dot luminance, and (2) modulations of dot density and modulations of dot contrast, in textures. The latter are much easier to detect when presented in phase with one another than when presented 180° out of phase, although out-of-phase modulations can also be detected given sufficient amplitude. This result supports the existence of two detection mechanisms: one that is excited by both density modulations and contrast modulations (quiescent when those modulations are presented 180° out of phase) and another that is relatively insensitive to either density modulations or contrast modulations (thus remaining stimulated regardless of phase angle). We investigate whether the mechanism responsible for detecting out-of-phase modulations depends on high-level computations (downstream from the confluence of monocular signals) or whether both mechanisms are situated at the monocular level of visual processing. Specifically, density-modulated and/or contrast-modulated stimuli were presented monocularly (i.e., to the same eye) or dichoptically (i.e., to opposite eyes). Out-of-phase modulations of density were much easier to detect when presented dichoptically. A dichoptic advantage was also found for out-of-phase density and contrast modulations. These dichoptic advantages imply conscious access to a mechanism at the monocular level of processing. When density modulations were presented dichoptically, 180° out of phase, detection thresholds were highest. Consequently, a mechanism with binocular input must also contribute to the detection of these modulations. We describe a minimal, image-based model for these results that contains one monocular computation and one binocular computation.

1. Introduction

The research described in this paper has three somewhat disparate antecedents. The first is a series of demonstrations (Kolb & Braun, 1995; Morgan, Mason, & Solomon, 1997; Solomon & Morgan, 1999; Solomon, John, & Morgan, 2006) that the modulation of textural properties (local orientation, in particular) can remain visible in brief, "inverse-cyclopean" displays. Such displays are inherently dichoptic. To qualify as inverse cyclopean (Julesz, 1971), the targets they contain must become invisible when the two eyes' displays are superimposed outside the visual system (and thus presented dioptically rather than dichoptically; see Fig. 1). These demonstrations unambiguously imply that there is a mechanism sensitive to textural modulations present at the monocular level of visual processing.

The second antecedent is Mulligan and MacLeod's (1988) report of reciprocity between density and luminance in textures composed of dots. Spatial modulations of density and luminance were difficult to detect when more-dense regions coincided with less-bright regions. The third and final noteworthy antecedent to the present material was Solomon and Morgan's (2020) signal-detection model for detecting and discriminating modulations of blur from modulations of contrast.

In an attempt to draw these latter two antecedents together, Morgan, MacLeod, and Solomon (2022) applied the model of Solomon and Morgan (2020) to the results of a summation experiment, in which modulations of dot density were presented both in phase and 180° out of phase with modulations of dot contrast. Although the model's fit can be considered satisfactory, we must note that – unlike blur, which can be estimated by comparing high-frequency content with low-frequency content – there is no generally accepted mechanism by which density can be estimated independently from stimulus contrast. Consequently, some dissatisfaction with Solomon and Morgan's model remained because it simply assigned arbitrary gains to different dimensions of modulation.

Aside from its reliance on arbitrary gains, there is at least one notable

* Corresponding author.
E-mail address: kristina.zeljic@city.ac.uk (K. Zeljic).

https://doi.org/10.1016/j.visres.2023.108347
Received 7 October 2023; Received in revised form 1 December 2023; Accepted 12 December 2023
Available online 25 December 2023

aspect of the model described by Morgan et al. (2022): it contains the minimum number of detection mechanisms required for qualitative consistency with their summation results. In the first of those results, Morgan et al. reported that detection thresholds for in-phase modulations of dot density and dot contrast were 30 %–55 % lower than the thresholds for either modulation in isolation. This near-perfect summation is consistent with a single mechanism that is sensitive to both types of modulation. An additional mechanism, responding primarily to one or the other modulation, is implicated by the similarity between thresholds for out-of-phase modulations and those for either type of modulation in isolation. The model of Morgan et al. can be considered minimal, as it comprises these two mechanisms and no others.

The current project was designed to serve two purposes. We sought an image-based model that did not rely on arbitrary gains for density modulation and contrast modulation. Moreover, we wanted to satisfy our curiosity regarding the mechanisms subserving the detection of these modulations. If two modulations are detected more readily when presented dichoptically than when presented dioptically, at least one of those modulations must activate a mechanism with monocular input. Conversely, a mechanism with binocular input would be implicated if detection depended on the phase angle between dichoptically presented modulations.

2. Methods

Participants included two authors and two volunteers who were naïve with respect to the purpose of these experiments. All had normal or corrected-to-normal vision and no history of visual or vestibular sensory disorders. Participant KZ wore corrective contact lenses. The study was approved by City, University of London's Optometry Proportionate Review Research Ethics Committee.

2.1. Stimuli

Left and right eyes' images were presented separately on the two Pentile OLED screens within a Rift CV1 head-mounted display (HMD; Oculus VR, LLC, Irvine, California, USA). Each screen had a refresh rate of 90 Hz and a resolution of 1080 x 1200 pixels, where each pixel had an angular subtense of 5.4 arcmin. The HMD was connected to an Oculus-ready PC system (Intel Core i7-6700K, 4 GHz, 16 GB RAM, Nvidia GeForce GTX 970 4 GB). Stimulus presentation was controlled using MATLAB with the Oculus VR library in Psychtoolbox (Brainard, 1997).

Compound stimuli were created by placing dots on a notional checkerboard of 70 × 70 squares. Dots comprising one component were placed on the black squares, dots comprising the other component were placed on the red squares. A spatial modulation was applied to each component's contrast or density by manipulating dot contrast $c(x)$ or probability of placement $p(x)$ in the horizontal dimension x, and then rotating the entire texture by ±45°. The rotated texture was viewed through a notional, fixed, circular aperture with radius 15.7° of visual angle, which allowed a maximum of 70 dots along its diameter. A concentric white circle, with radius 22.2° of visual angle, remained visible throughout the experiment. Fig. 2 illustrates examples in which the two components were exposed to different eyes. In both examples, one component has a contrast modulation, the other has a density modulation.

The profile of each dot matched that of a bivariate normal density having covariance matrix:

$$\Sigma = \begin{bmatrix} (1\text{pixel})^2 & 0 \\ 0 & (1\text{pixel})^2 \end{bmatrix}.$$

Its polarity was bright or dark with equal probability, determined independently from that of every other dot. For components having a contrast modulation, a dot was placed in each (notionally black or red) square with a fixed probability of 0.5. The peak Weber contrast of each dot was a sinusoidal function of position:

$$c(x) = \pm[1 + m_c \cos(4\pi x + \varphi)]/2$$

In this expression x extends from –0.5 at the left edge of the aperture to

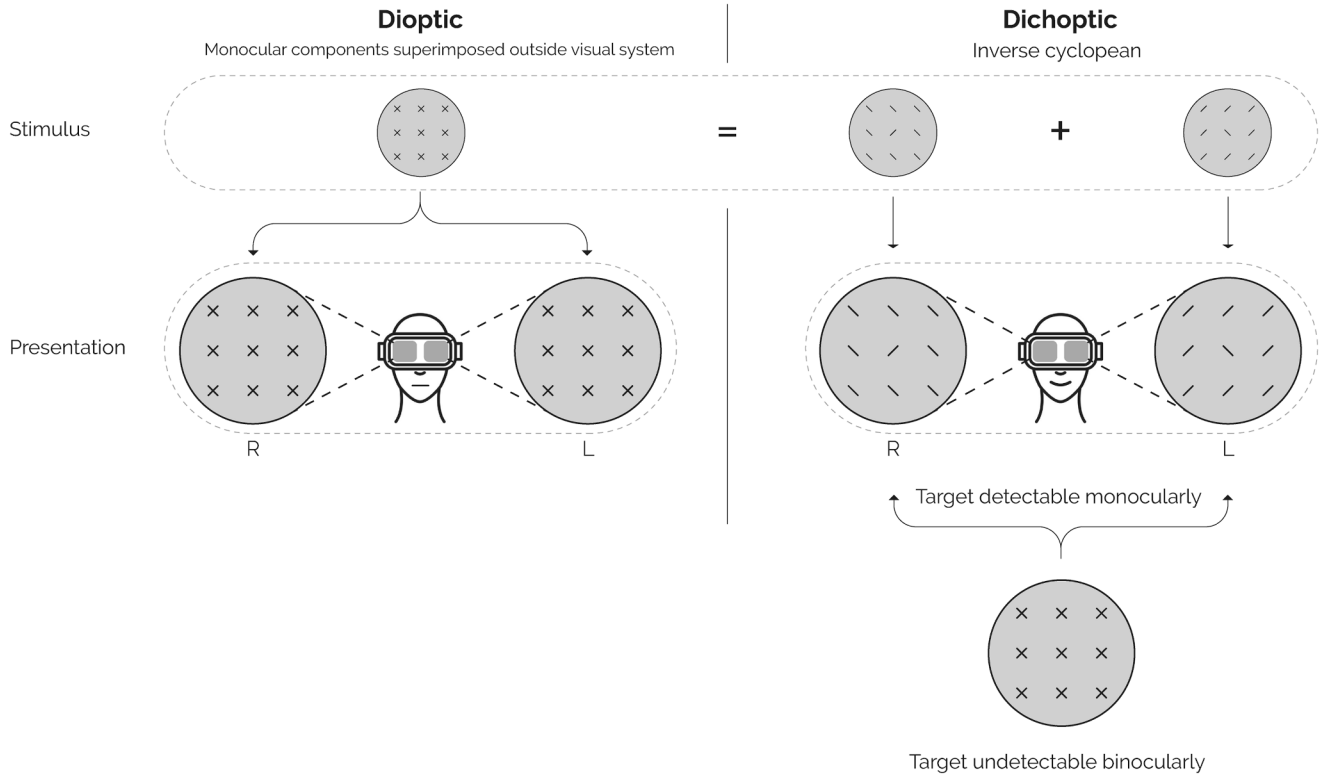

Fig. 1. Dioptic (left), and dichoptic, inverse-cyclopean (right) displays.

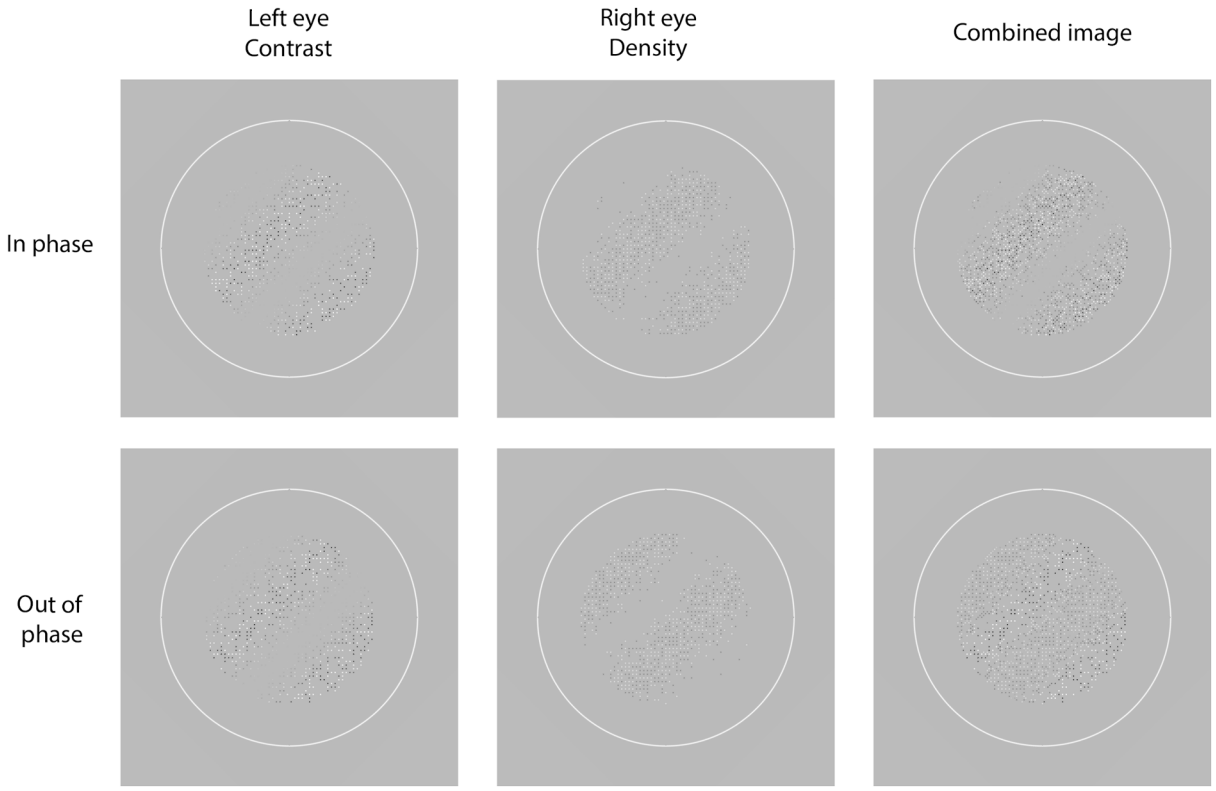

Fig. 2. Example stimuli showing how individual components (contrast: left; density: centre) at maximum modulation amplitude are combined in phase (top row) and out of phase (bottom row).

0.5 at the right edge. Thus, there are two complete cycles of modulation. Unless otherwise constrained (see below), the spatial phase φ was selected at random from the set $\{0, 90^{\circ}, 180^{\circ}, 270^{\circ}\}$. Modulation amplitude m_c was determined by an adaptive staircase, described below (Experiment 2).

For components having a density modulation, the peak Weber contrast of each dot was fixed at ± 0.5. A dot was placed in each (notionally black or red) square with probability

$$p(x) = [1 + m_d \cos(4\pi x + \varphi)]/2$$

Where the modulation amplitude m_d was determined by an adaptive staircase and the spatial phase φ was selected at random from the set $\{0, 90^{\circ}, 180^{\circ}, 270^{\circ}\}$, unless otherwise constrained, as described below (Experiment 2).

2.2. Procedure

Participants were seated in front of the table in a height-adjustable chair in a quiet, darkened room. They donned the HMD and were instructed to tighten the straps to secure it. The experimenter then asked the participant to confirm that the HMD was fitted comfortably, and the view of the test stimulus was in focus. Textured tape was attached to the response keys so that they could be identified haptically. On each trial, a contrast-modulated and/or density-modulated texture was presented for 0.5 s, accompanied by an auditory click. The participant pressed a response key to indicate whether it was tilted leftward or rightward (i.e., rotated $\pm 45^{\circ}$ with respect to vertical). Guess rate – i.e., accuracy in the limit, as the modulation amplitude approaches zero – for this task is $\gamma = 0.5$. Lapse rates δ were estimated for each participant from a randomly selected subset of trials (10 % of the total), in which the adaptive staircase was ignored in favour of the maximum modulation amplitude.

2.3. Experiment 1

Experiment 1 was designed to determine thresholds for each component texture, when viewed monocularly, in isolation. A QUEST staircase (Watson & Pelli, 1983) converged on the modulation amplitude required for participants to achieve 81 % accuracy in each of four conditions: left-eye contrast, right-eye contrast, left-eye density, and right-eye density. These conditions were randomly interleaved in a block of 200 trials, with each participant completing a minimum of two blocks.

For our threshold estimates, we used the scale parameter α from the log-Weibull function, compressed to the range $(\gamma, 1 - \delta)$, which best-fit the response frequencies in each condition. These maximum-likelihood fits were obtained with best-fitting (maximum likelihood) values of β for each participant in each condition. This parameter determines the slope of the psychometric function. See Fig. A1 and Table A1 for further details.

2.4. Experiment 2

Experiment 2 was designed to determine performance with compound textures, in which two monocularly exposed components (one on the notionally black squares and one on the notionally red squares) were presented at equal multiples of their thresholds, as determined in Experiment 1. A QUEST staircase converged on the multiple of threshold required for participants to achieve 81 % accuracy in each of 16 conditions:

1. Left-eye contrast and left-eye density out of phase
2. Left-eye contrast and left-eye density in phase
3. Right-eye contrast and right eye density out of phase
4. Right-eye contrast and right-eye density in phase
5. Left-eye contrast and right-eye density out of phase

6. Left-eye contrast and right-eye density in phase
7. Right-eye contrast and left-eye density out of phase
8. Right-eye contrast and left-eye density in phase
9. Right-eye contrast and right-eye contrast in phase
10. Left-eye contrast and left-eye contrast in phase
11. Right-eye density and right-eye density in phase
12. Left-eye density and left-eye density in phase
13. Right-eye contrast and left-eye contrast out of phase
14. Right-eye contrast and left-eye contrast in phase
15. Right-eye density and left-eye density out of phase
16. Right-eye density and left-eye density in phase

This list excludes the following 4 out of the total 20 logical combinations of eye (left and/or right), modulation (contrast and/or density) and phase (in phase or out of phase):

17. Right-eye contrast and right-eye contrast out of phase
18. Left-eye contrast and left-eye contrast out of phase
19. Right-eye density and right-eye density out of phase
20. Left-eye density and left-eye density out of phase

Although the modulations in excluded conditions 19 and 20 were necessarily invisible, the modulations in excluded conditions 17 and 18 might not have been invisible. This is because each component modulation was applied to a distinct set of dots. Participants JAS and KZ completed a total of 4 blocks of 400 trials each, resulting in a total of 100 trials per condition. Participant RDS completed 2 blocks, for a total of 50 trials per condition. Participant DVD completed 5 blocks, yielding 100–150 trials per condition.

3. Results

Raw data and analyses thereof for each individual participant can be found in the Appendix (See Fig. A2). Mean threshold elevations across all 4 participants are illustrated at the top of Fig. 3. Each threshold elevation is the difference (in dB) between threshold for the compound modulation, as measured in Experiment 2, and threshold for each isolated modulation, as measured in Experiment 1. Negative threshold elevations correspond to threshold reductions.

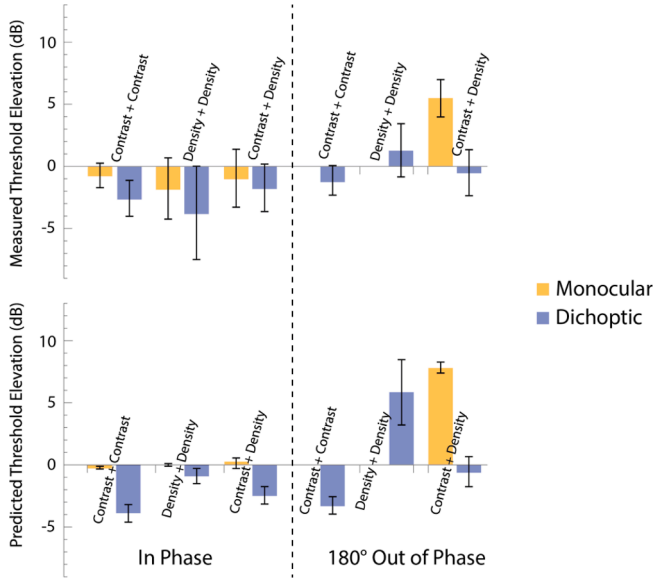

Fig. 3. Detection thresholds (mean ± 1 SD, $N = 4$) for 2-component dot textures. Thresholds are expressed as multiples of the corresponding thresholds for isolated components, in dB (i.e., where 6 dB corresponds to a factor of 2). Our image-based model can produce threshold elevations (bottom) similar to those derived from atheoretical Weibull fits (top), including i) dichoptic advantages in the out-of-phase conditions, ii) an effect of phase angle when two density modulations are presented dichoptically, and iii) zero threshold elevation when component modulations are presented in phase to the same eye.

We found a distinct dichoptic advantage for out-of-phase (but equally visible) modulations of density and contrast. That is, threshold was lower [6.0 dB ± 1.5 dB; $t(3) = 7.97$, $p = 0.002$] when the two components were presented to different eyes than when they were presented to the same eye. The results also indicate a dichoptic advantage for detecting two out-of-phase density modulations. (Were those modulations presented to the same eye, they would have been invisible.) Consequently, the results strongly imply the existence of at least one mechanism sensitive to density modulations at the monocular level of processing.

Our results also contain evidence for an effect of phase angle [5.0 dB ± 3.5 dB; $t(3) = 2.86$, $p = 0.032$] on thresholds for dichoptic Density + Density compounds. This suggests a mechanism that receives input from both eyes. No effect of phase angle would be expected if it received merely monocular input.

Note that there was no significant threshold elevation (positive or negative) for monocular compounds when their two component modulations were presented in phase with one another. *Prima facie* this may seem inconsistent with the reduction in threshold for in-phase modulations of contrast and density reported by Morgan et al. (2022). However, Morgan et al. applied contrast and density modulations to a single set of dots. Dichoptic stimulation in the current experiment, on the other hand, necessitates modulation of different dots in the two eyes. Fair comparison, therefore, likewise necessitates component modulations of different dots in our monocular conditions. The lack of significant threshold elevation (positive or negative) in these conditions means that a modulation's detectability remained unaffected after doubling the product between density and contrast at both its peak and its trough. This final result can be considered consistent with Weber's Law.

4. An image-based model for detecting modulations of dot density and dot contrast

Although the model described by Morgan et al. (2022) can be modified to produce data similar to those collected in these dichoptic experiments, it cannot explain how density modulations become partially disentangled from contrast modulations. One potential process is described below: an expansive nonlinearity applied to each dot can disproportionately increase the impact of higher contrasts, whereas a compressive nonlinearity can reduce the difference between impacts of high-contrast and low-contrast dots, thereby creating a signal largely based on dot density. Although, for simplicity, both mechanisms in the model employ power-function nonlinearities, we placed no constraints on their exponents, whose values were allowed to vary independently when fitting the model to data.

Inputs to the model were stimuli similar to those described in the Methods section. However, circular apertures were not used, and image orientations were horizontal or vertical, rather than ±45°. The full imaging pipeline is shown in Fig. 4. In the monocular channel, transformations are applied separately to the image in each eye. In the other, binocular channel, summation of the two eyes' images is computed before the following transformations. First, full-wave rectification is applied to each pixel's Weber contrast (Weber contrasts are approximately proportional to the output from a high-pass, linear filter; Dakin, Tibber, Greenwood, Kingdom, & Morgan, 2011). Next, a pointwise, nonlinear transformation is applied to each rectified stimulus. To get a phase-independent visual signal, we use quadrature pairs. Dot products between the full-wave rectified, transduced stimulus and quadrature pairs that are perpendicular to each other (one pair tuned to horizontal targets, the other tuned to vertical targets) are computed. To obtain Weber's Law, each dot product is normalised by the sum of a small constant and the dot products between these outputs and full-wave rectified versions of the quadrature pairs. For steep psychometric

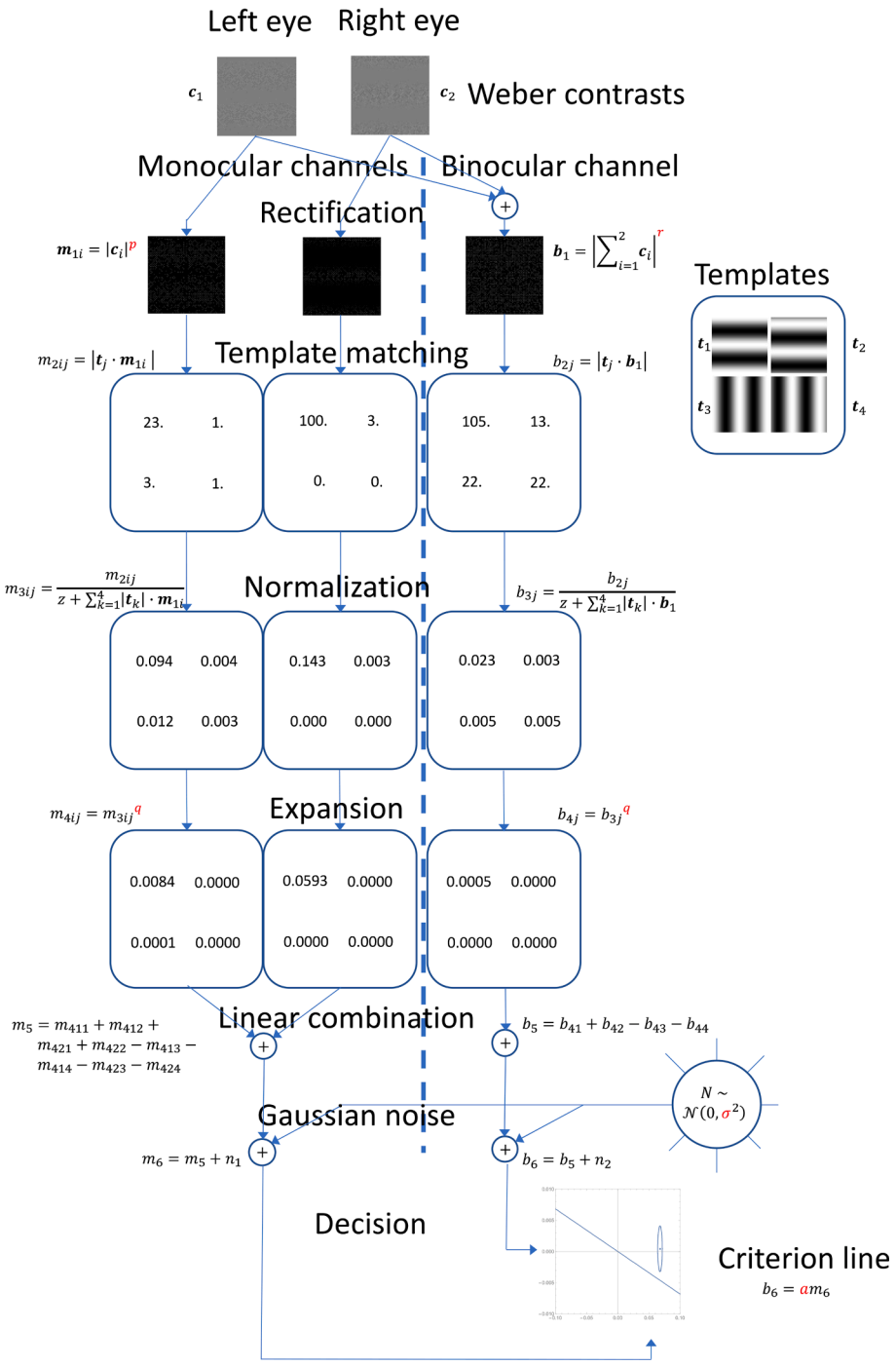

Fig. 4. Imaging pipeline. Left-eye and right-eye images are matrices of Weber contrast. In this example, images contain dichoptic, out-of-phase modulations of density (left eye) and contrast (right eye), 9 dB above participant JAS's detection thresholds for each eye's modulation in isolation. Image resolution (210 × 210) is somewhat smaller than that used in the actual experiment. The binocular channel receives the sum of the two eyes' images. At the first stage of processing, images undergo pointwise, nonlinear, full-wave rectification, adhering to a power law with exponents p and r in the monocular and binocular channels, respectively. (When drawn around a bold-face character denoting a matrix, vertical bars signify a pointwise or element-by-element transformation, whose result is a matrix of the same size.) The model's 5 free parameters appear in red. At the second stage of processing, each signal is matched with two quadrature pairs of sinusoidal templates. At the third stage, each of these matches (a dot product) is normalized by something like contrast energy. Specifically, we use the sum of a small constant ($z = 10^{-8}$) to prevent divide-by-zero errors and the dot products between the rectified stimuli and similarly rectified versions of the quadrature pairs. This normalization produces near-zero monocular threshold elevations. At the fourth stage of processing, each signal undergoes another (expansive) nonlinear transformation. This expansion (a power law, with exponent $q > 1$) produces steep psychometric functions. At the fifth stage of processing, signals in the monocular and binocular channels are combined linearly to produce deterministic, scalar values. At the sixth stage, an independent sample of zero-mean, Gaussian noise is added to each channel. Its variance is σ^2. The ellipse represents 1 standard deviation of the noise in every direction around this example's mean in the plane of all possible monocular and binocular signals. A criterion line segregates the plane of all possible signals into those favouring horizontal and those vertical horizontal targets. The gradient of this criterion (a) effectively determines the relative weight of monocular and binocular signals in the decision process. For this example, we use parameter values fit to the data from participant JAS ($p = 3.6$, $r = 0.44$, $q = 2.0$, $\sigma = 0.0037$, and $a = -0.07$). (For interpretation of the references to colour in this figure legend, the reader is referred to the web version of this article.)

functions (see Table A1), expansive transduction is applied to each normalized dot product. Next, a comparison (subtraction) between the two sums of each quadrature pair is carried out for each of the channels. An independent sample of zero-mean, Gaussian noise is then added. The relative weight of monocular and binocular signals in the decision process is determined by the gradient of a criterion line that segregates the plane of all possible monocular and binocular signals into those favoring horizontal targets and those favoring vertical targets.

For each depth of modulation selected by the QUEST staircases (see Methods) in each of the 20 conditions in Experiments 1 and 2, we calculated the model's predicted accuracy using 10 randomly generated stimuli. Mathematica's FindMinimum routine converged upon the parameter values that maximised the joint likelihood of a participant's actual accuracies, given the model's predictions.[1] This optimisation routine was repeated with the results from each participant. Model code and fitting details can be found in the Supplementary Material.

Fig. 3 (bottom) shows mean threshold elevation predicted by the model for all participants in each condition and Table 1 contains best-fitting parameter values and log likelihood for each participant.

For all four participants, best fits were obtained when the monocularly driven mechanism employed an expansive point-wise nonlinearity ($p \gg 1$). Consequently, modulations of dot contrast had a greater impact on monocular signals than modulations of dot density. For all four observers, best fits were obtained when the binocularly driven mechanism employed a compressive point-wise nonlinearity ($r \ll 1$). Consequently, modulations of dot density had a greater impact on binocular signals than modulations of dot contrast.

One of the things to notice in Fig. 2 (bottom) is that the model predicts no threshold elevation (positive or negative) for monocular compounds when their two component modulations were presented in phase with one another. Without a normalization stage the model would have been incapable of producing this result, consistent with Weber's Law for contrast energy and thus density. Another thing to notice is that, whereas the model predicts a large effect of phase angle on dichoptic Density + Density compounds, it doesn't predict a large effect of phase angle on dichoptic Contrast + Contrast compounds. This difference can be attributed directly to the difference in power-function exponents. In the binocular channel, the exponent is compressive, emphasizing the impact of density modulations over contrast modulations. In the monocular channel, we have the reverse: an expansive exponent, emphasizing the impact of contrast modulations over density modulations. One final thing to notice is that the model predicts a large dichoptic advantage for out-of-phase compounds of Contrast + Density. Without a monocular channel, this dichoptic advantage would have been impossible.

Although the model has proven to be quite successful in producing results qualitatively similar to those of our human participants, it is far from perfect. Perhaps the largest quantitative discrepancy occurred in the Dichoptic Density + Density condition. Best fits were obtained when the model predicted 3.4 dB or more threshold elevation for each observer. However, threshold elevation in this condition proved significant for only one of our four observers (RDS, see Fig. A2).

Table 1
Parameter values maximizing the likelihood of the model fit to the psychometric functions.

Participant	p	r	q	σ	a	$\ln L$
JAS	3.6	0.44	2.0	0.0037	−0.07	−1118.2
KZ	2.2	0.22	1.8	0.0064	−0.33	−1110.7
RDS	2.2	0.24	1.3	0.0414	−0.39	−666.0
DVD	4.0	0.64	1.2	0.0488	−0.22	−1038.9

[1] A 2020 MacBook Pro with Apple's M1 microprocessor was capable of computing expected accuracy for a given stimulus in approximately 0.03 s. Thus, given one set of parameter values, it could calculate the joint likelihood of one participant's actual accuracies in approximately 14 min (7 min for RDS). For each participant, several days were required for FindMinimum to converge (within a specified accuracy of two decimal places) on the five parameter values maximising this joint likelihood.

5. Discussion

From our empirical findings, we can safely draw two general conclusions. 1) Dichoptic advantages for detecting 180° out-of-phase modulations of dot contrast and/or dot density imply that there must be at least one mechanism sensitive to these modulations at the monocular level of visual processing. 2) The relative ease with which in-phase, dichoptic modulations of density can be detected, as compared with 180° out-of-phase, dichoptic modulations, implies at least one mechanism sensitive to these modulations at the binocular level of visual processing.

Given these constraints, we have assembled a relatively simple, image-based model capable of producing data similar to those from our human participants. As with the model envisioned by Durgin and Proffitt (1996), ours employs different non-linearities for dissociating signals similar to contrast energy from signals similar to texture density. Furthermore, our model incorporates their proposal that both of these signals act as input to a texture-discrimination process.

Whereas Durgin and Proffitt (1996) noted that a (compressive) nonlinearity could produce visual signals commensurate with texture density, Zavitz and Baker (2013, 2014) actually constructed an image-based model, wherein this compression subserved texture segregation on the basis of density as well as the influence of density on the visibility of other textural differences. Conversely, Morgan, Raphael, Tibber, and Dakin (2014) described an image-based model of density discrimination, in which the influence of contrast variability was minimized with a simple, compressive transformation of (unsigned) image contrast.

One notable aspect of our model's simplicity is the similarity between its monocular and binocular mechanisms. The only difference between these mechanisms, other than the fact that monocular mechanisms get input from one eye and binocular mechanisms get input from two eyes, lies in the value of the exponent defining the power-function related input to output. Indeed, it might be worth noting that these two exponents, a third parameter describing the relative weight of monocular and binocular signals in the decision process, and a fourth parameter defining the performance-limiting noise were the only free parameters in an even simpler model which proved incapable of producing data consistent with Weber's Law for density.

It should be noted that, although our data are consistent with Weber's Law for density (i.e., a threshold elevation equal to 0 for in-phase, monocular, density + density compounds), we must refrain from accepting this null hypothesis, especially considering evidence to the contrary, such as that collected by Burgess and Barlow (1983), who used a very different psychophysical paradigm (participants were required to detect the boundary of a bi-partite field). Nonetheless, to produce data similar to those from our human participants, our otherwise relatively simple model was forced to incorporate computations at least approximately consistent with Weber's Law. Given the fact that nonlinear transduction had already been incorporated into both our model's mechanisms, we opted for divisive inhibition (Foley, 1994).

Although successful in producing near-zero threshold elevations for in-phase, monocular, compound modulations, one inescapable by-product of divisive inhibition is a flattening of the psychometric function of probability correct vs. log modulation depth. Consequently, one final, additional stage of signal processing was required for the model to produce psychometric functions that weren't implausibly shallow. The simplest such computation seemed to be a late-stage, expansive nonlinearity. Again, we opted for a power-function, whose exponent became the fifth (of five) free parameters in the image-based model that

we describe as 'minimal', even if it has 6 distinct processing stages (see Fig. 4)!

Interocular transfer (and the lack thereof) of adaptation to textures having various densities and contrast energies allowed Durgin (2001) to infer a monocular mechanism sensitive to contrast energy and a binocular mechanism sensitive to density. Our results confirm and extend these findings. Whereas the possibility of monocular gain-control circuits precludes safe inferences regarding conscious access to monocular signals from incomplete interocular transfer of adaptation-induced sensitivity changes (Georgeson, Lerner, & Kingdom, 2023), such inferences can be made from the dichoptic advantages reported here. These advantages imply that the texture-segregation processes receive input from neurons with monocular (or otherwise unbalanced) input.

CRediT authorship contribution statement

Kristina Zeljic: Conceptualization, Data curation, Formal analysis, Investigation, Methodology, Project administration, Resources, Software, Visualization, Writing – original draft. **Michael J. Morgan:** Conceptualization, Data curation, Funding acquisition, Investigation, Methodology, Resources, Supervision, Writing – review & editing. **Joshua A. Solomon:** Conceptualization, Software, Validation, Investigation, Resources, Methodology, Formal analysis, Visualization, Supervision, Project administration, Writing – review & editing.

Declaration of competing interest

The authors declare that they have no known competing financial interests or personal relationships that could have appeared to influence the work reported in this paper.

Data availability

Supplementary Material is available online at www.staff.city.ac.uk/~solomon/ConDensDichop.zip.

Acknowledgments

KZ, JAS, and MJM receive support from the Leverhulme Trust (grant #RPG-2021-020).

The authors thank Teodor Cozma for his assistance on Fig. 1.

Appendix

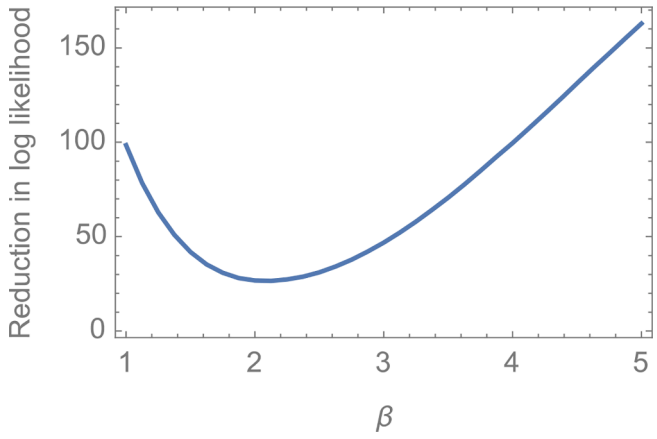

Fig. A1. Reductions in goodness-of-fit. The Weibull distribution was separately fit to 48 psychometric functions (12 conditions/observer × 4 participants) of probability correct vs. log modulation depth. Maximum, joint (base-10) log likelihood was –423. Fixing the Weibull shape parameter β caused likelihoods to fall by the amounts indicated. The reduction in likelihood was minimal when β was fixed at the value of 2.09. Note that $\Delta AIC = -94 + 26.50 \ln 100 = 28.1$, providing "essentially no support" (Burnham & Anderson, 2003, p. 70) for the nested model with a fixed value for β. Neither allowing β to vary with participant (but not condition) nor condition (but not participant) helps ($\Delta AIC = 23.9$ and $\Delta AIC = 20.6$, respectively).

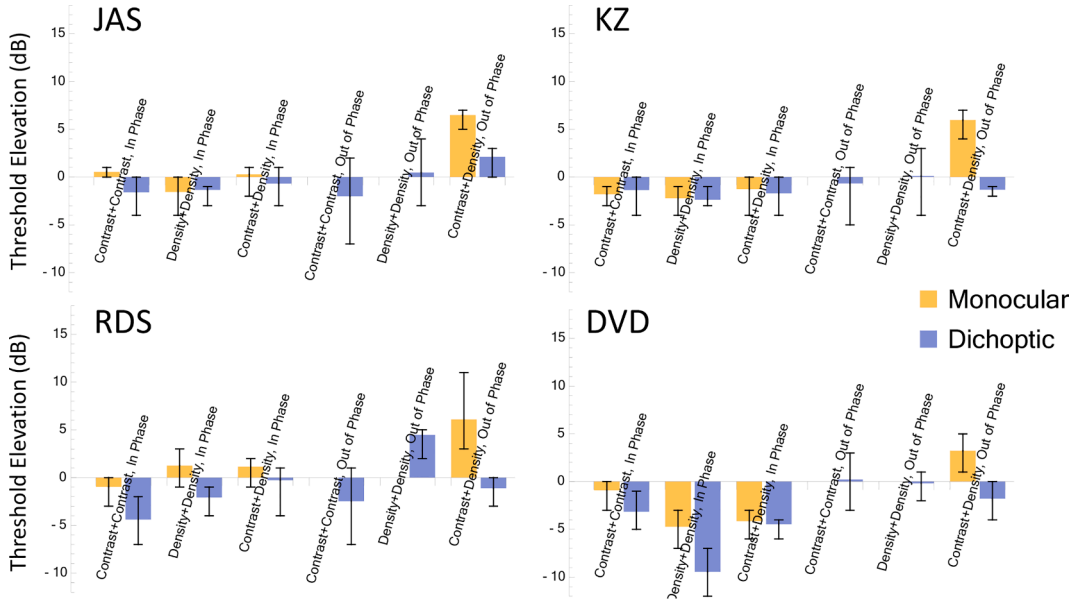

Fig. A2. Detection thresholds for 2-component dot textures. Thresholds are expressed as multiples of the corresponding thresholds for isolated components, in dB. Error bars contain 95% credible intervals.

Table A1
Best-fitting (maximum likelihood) values of β for each participant in each condition. Values at the end of each row and/or column are best-fitting values for all participants and/or conditions.

	JAS	KZ	RDS	DVD	All
1-component contrast	3.41	2.02	2.80	1.98	2.38
1-component density	2.03	1.25	1.77	1.74	1.84
Monocular contrast + contrast in phase	2.72	2.04	1.31	1.47	1.81
Dichoptic contrast + contrast in phase	1.59	3.09	4.62	3.43	2.22
Monocular density + density in phase	1.61	2.41	1.79	2.01	1.90
Dichoptic density + density in phase	3.21	3.74	5.95	3.01	3.65
Monocular contrast + density in phase	2.80	2.70	3.16	1.80	2.23
Dichoptic contrast + density in phase	1.88	1.25	4.43	2.59	2.45
Monocular contrast + density out of phase	2.46	2.53	1.36	1.20	1.87
Dichoptic contrast + density out of phase	3.18	5.41	5.34	1.16	1.99
Dichoptic contrast + contrast out of phase	1.12	3.20	1.93	2.72	1.75
Dichoptic density + density out of phase	2.08	1.98	6.06	4.68	3.38
All conditions	2.21	2.59	2.01	1.81	2.09

References

Burgess, A., & Barlow, H. B. (1983). The precision of numerosity discrimination in arrays of random dots. *Vision Research, 23*, 811–820.

Burnham, K. P., & Anderson, D. R. (2003). *Model Selection and Multimodel Inference: A Practical Information-Theoretic Approach*. Springer Science & Business Media.

Dakin, S. C., Tibber, M. S., Greenwood, J. A., Kingdom, F. A., & Morgan, M. J. (2011). A common visual metric for approximate number and density. *Proceedings of the National Academy of Sciences of the United States of America, 108*, 19552–19557.

Durgin, F. H. (2001). Texture contrast aftereffects are monocular; texture density aftereffects are binocular. *Vision Research, 41*, 2619–2630.

Durgin, F. H., & Proffitt, D. R. (1996). Visual learning in the perception of texture: Simple and contingent aftereffects of texture density. *Spatial Vision, 9*, 423–474.

Foley, J. M. (1994). Human luminance pattern mechanisms: masking experiments require a new model. *Journal of the Optical Society of America. A, 11*, 1710–1719.

Georgeson, M., Lerner, P., & Kingdom, F. (2023). Binocular properties of contrast adaptation in human vision. *Vision Research, 209*, Article 108261.

Kolb, F. C., & Braun, J. (1995). Blindsight in normal observers. *Nature, 377*(6547), 336–338.

Morgan, M. J., MacLeod, D. I., & Solomon, J. A. (2022). The channel for detecting contrast modulation also responds to density modulation (or vice versa). *Vision Research, 192*, Article 107948.

Morgan, M. J., Mason, A. J. S., & Solomon, J. A. (1997). Blindsight in normal subjects. *Nature, 385*(6615), 401–402.

Morgan, M. J., Raphael, S., Tibber, M. S., & Dakin, S. C. (2014). A texture-processing model of the 'visual sense of number'. *Proceedings of the Royal Society B: Biological Sciences, 281*, 20141137.

Mulligan, J. B., & MacLeod, D. I. (1988). Reciprocity between luminance and dot density in the perception of brightness. *Vision Research, 28*, 503–519.

Solomon, J. A., John, A., & Morgan, M. J. (2006). Monocular texture segmentation and proto-rivalry. *Vision Research, 46*, 1488–1492.

Solomon, J. A., & Morgan, M. J. (1999). Dichoptically cancelled motion. *Vision Research, 39*, 2293–2297.

Watson, A. B., & Pelli, D. G. (1983). QUEST: A Bayesian adaptive psychometric method. *Perception and Psychophysics, 33*, 113–120.

Zavitz, E., & Baker, C. L. (2013). Texture sparseness, but not local phase structure, impairs second-order segmentation. *Vision Research, 91*, 45–55.

Zavitz, E., & Baker, C. L. (2014). Higher order image structure enables boundary segmentation in the absence of luminance or contrast cues. *Journal of Vision, 14*(4), 14.